Frequency-Domain Modeling-Free Iterative Learning Control for Point-To-Point Motion

1st Yoshihiro Maeda
Electrical and Mechanical Engineering Program
Department of Engineering
Nagoya Institute of Technology
Nagoya, Japan
ymaeda@nitech.ac.jp

2nd Makoto Iwasaki
Electrical and Mechanical Engineering Program
Department of Engineering
Nagoya Institute of Technology
Nagoya, Japan
iwasaki@nitech.ac.jp

***Abstract*—The data-driven autonomous feedforward (FF) control design technique known as frequency-domain modeling-free iterative learning control (MFILC) has gained attention for its ability to achieve fine motion control performance without excessive labor. However, the existing frequency-domain MFILC methods that rely on empirical transfer function estimation are not suitable for point-to-point (PTP) motion due to the leakage error that occurs in frequency response function (FRF) estimation. To address this issue, this study proposes an improved frequency-domain MFILC method that employs the differential filtering-based empirical transfer function estimation for FRF estimation. This enhancement enables the proposed method to learn the FF compensation in both reciprocating and PTP motion. Simulations were conducted to evaluate the effectiveness of the proposed method in achieving fast and precise motion control of a galvano scanner.**

***Index Terms*—modeling-free iterative learning control, frequency responses function, empirical transfer function estimation with differential filtering, feedforward compensation.**

I. Introduction

The implementation of feedforward (FF) compensation via two-degree-of-freedom (2DoF) control has proven to be a successful strategy for achieving fast and precise motion control in various industrial mechatronic systems, including semiconductor manufacturing machines, electronics equipment machines, and machine tools [1], [2]. It is widely recognized that model-based FF compensation is one of the optimal approaches for achieving precise tracking performance with respect to a target reference [3]–[5]. However, the identification of target system characteristics and the construction of a precise parametric model for developing high-performance FF compensation necessitate expert-level proficiency and considerable effort [6], [7].

As one of the data-driven autonomous FF design approaches, modeling-free iterative learning control (MFILC) [5], [8] is promising to overcome the aforementioned problem. Recently, significant research efforts have been devoted to frequency-domain inversion-based MFILC [9]–[12] which boasts several advantages such as stable inversion implementation and elimination of the need for persistently exciting signals. Notably, this approach has been extended to nonlinear systems [13] and MIMO systems [14]. The frequency-domain MFILC approach involves implementing the inversion of system dynamics as a frequency response function (FRF) derived from time-domain system input and output data through the discrete Fourier transform (DFT) during repetitive motion. The empirical transfer function estimation (ETFE) method is the most commonly used approach for FRF estimation due to its ease of use and implementability in industrial machines [6]. However, conventional frequency-domain MFILC methods are limited to reciprocating motion to circumvent FRF estimation errors resulting from DFT-induced leakage. Since repetitive motion in industrial machines encompasses not only reciprocating motion but also point-to-point (PTP) motion, extending the learning conditions is critical.

This study proposes an improved frequency-domain MFILC method that is applicable to both reciprocating and PTP motion, as efficient automated FF design. The proposed method builds upon the conventional MFILC approach [10], with the exception of the ETFE method, which is replaced with the differential filtering-based ETFE (ETFE-Diff) [15], [16] to mitigate FRF estimation errors resulting from leakage. The contributions of this study are summarized as follows.

1) Presents a novel algorithm for the proposed MFILC approach, which employs ETFE-Diff-based FRF estimation, and provides a theoretical explanation of the principle of stable learning in PTP motion. A comparison of this approach with conventional ETFE-based MFILC [10] is also presented.
2) Simulation evaluations were conducted to demonstrate the effectiveness of the proposed MFILC approach. The results showed that the proposed approach can successfully design FF compensation with monotonic convergence even in PTP motion, resulting in fast and precise position tracking performance that outperforms the conventional method.

The simulation evaluations were performed using a galvano scanner, which is an example of an industrial servo system

This work was supported by The MAZAK Foundation and JSPS KAKENHI (grant number 20K04545). The authors would like to thank Via Mechanics, Ltd, for providing the experimental equipment.

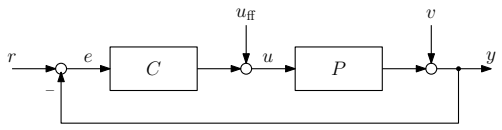

Fig. 1. Representation of 2DoF control system.

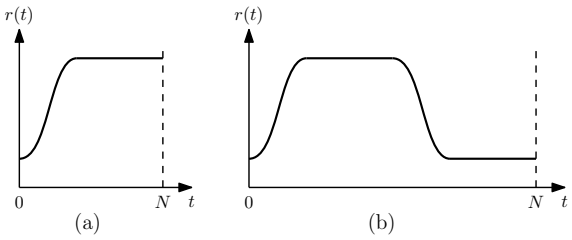

Fig. 2. Conceptual waveforms of reference $r(t)$: (a) PTP motion; (b) reciprocating motion.

used in printed circuit board laser processing machines. From this point forward, the frequency-domain MFILC approach will be referred to simply as MFILC.

II. Problem Formulation

Consider a 2DoF control system shown in Fig. 1, where P is the plant, C is the feedback (FB) controller, r is the reference, u is the control input, y is the control output, $u_{\rm ff}$ is the FF control input, $e(= r - y)$ is the error, and v is the disturbing noise, respectively. P and C are the linear time-invariant discrete-time systems. The state-space expression of P is described as follows:

$$\begin{aligned} \boldsymbol{x}_{\rm p}(t+1) &= \boldsymbol{A}_{\rm p}\boldsymbol{x}_{\rm p}(t) + \boldsymbol{B}_{\rm p}u(t) \\ y(t) &= \boldsymbol{C}_{\rm p}\boldsymbol{x}_{\rm p}(t) + v(t) \end{aligned} \tag{1}$$

where $\boldsymbol{x}_{\rm p}(t) \in \mathbb{R}^{n_{\rm p}}$ is the state vector at a discrete time t, and $\boldsymbol{A}_{\rm p} \in \mathbb{R}^{n_{\rm p}\times n_{\rm p}}$, $\boldsymbol{B}_{\rm p} \in \mathbb{R}^{n_{\rm p}}$, and $\boldsymbol{C}_{\rm p} \in \mathbb{R}^{1\times n_{\rm p}}$ are the state matrices.

The objective of this study is to automatically design the FF control input $u_{\rm ff}$ such that y precisely follow to r by repeating PTP motion. The detailed conditions in the FF design problem are stated as follows:

- C1: The reference $r(t)$ is a fixed, smooth, and PTP waveform as shown in Fig. 2(a).
- C2: The N-point finite-length time-domain data $r(t)$, $u_{\rm ff}(t)$, $u(t)$, $y(t)$, and $e(t)$, $t = 0, 1, \ldots, N-1$ can be used for the FF design.
- C3: The dynamics of plant P are *unknown* and modeling of P with a parametric model is not performed.
- C4: A PTP motion starts from and ends to settled states, that is,

$$\begin{aligned} \boldsymbol{x}_{\rm p}(t \le -1) &= \boldsymbol{x}_{\rm p}(0) \\ \boldsymbol{x}_{\rm p}(t \ge N) &= \boldsymbol{x}_{\rm p}(N-1) \end{aligned} \tag{2}$$

In this study, DFT of a time-domain data $x(t), t = 0, 1, \ldots, N-1$ is defined as

$$X(k) = \sum_{t=0}^{N-1} x(t) e^{-j\frac{2\pi kt}{N}}, \ k = 0, 1, \ldots, N-1 \tag{3}$$

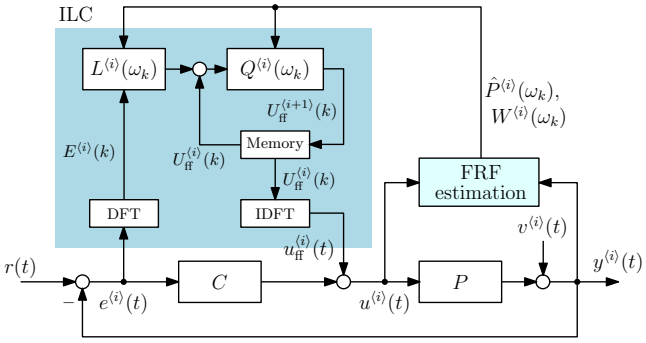

Fig. 3. Block diagram of MFILC.

where the frequency index k corresponds to the frequency $\Omega_k = 2\pi k/(NT_{\rm s})$ with the sampling time $T_{\rm s}$.

III. Frequency-Domain Modeling-Free Iterative Learning Control (MFILC)-Based FF Design

The proposed MFILC is based on the conventional MFILC [10], which is designed for reciprocating motion as shown in Fig. 2(b). By applying the ETFE-Diff approach, the proposed MFILC approach extends the conventional MFILC to enable stable learning of the FF control input in PTP motion, as shown in Fig. 2(a). In the following sections, we first present the overall algorithm of the proposed MFILC-based FF design and provide an explanation of the fundamental theory of MFILC. Then, we describe the principle of ETFE-Diff-based FRF estimation, with a focus on the leakage error that arises in PTP motion. This is compared to the ETFE-based FRF estimation method used in the conventional MFILC approach.

A. Autonomous FF Design Algorithm

Fig. 3 shows the block diagram of MFILC, where $\langle i\rangle$ is the symbol expressing i-th learning iteration, $L^{\langle i\rangle}(\omega_k)$ is the learning filter, $Q^{\langle i\rangle}(\omega_k)$ is the robustness filter for stabilizing the learning process against the FRF estimation error or disturbing noise, $\hat{P}^{\langle i\rangle}(\omega_k)$ is the plant FRF estimate, $W^{\langle i\rangle}(\omega_k)$ is the reliability function expressing the reliability of $\hat{P}^{\langle i\rangle}(\omega_k)$, $E^{\langle i\rangle}(k)$ is the DFT of $e^{\langle i\rangle}(t)$, and $U_{\rm ff}^{\langle i\rangle}(k)$ is the DFT of $u_{\rm ff}^{\langle i\rangle}(t)$. Note that the ILC part is calculated in frequency-domain via DFT and inverse discrete Fourier transform (IDFT). Fig. 4 shows the flowchart of autonomous FF design algorithm and processes in each step are summarized as follows:

Step 1: Initialize the learning iteration counter i to $i = 0$.

Step 2: Perform a PTP motion using the control system shown in Fig. 3 and obtain the N-point time-domain data $e^{\langle i\rangle}(t)$, $u_{\rm ff}^{\langle i\rangle}(t)$, $u^{\langle i\rangle}(t)$, and $y^{\langle i\rangle}(t)$.

Step 3: If i equals to the end learning iteration times $N_{\rm lrn}$, then end learning and obtain $u_{\rm ff}^{\langle N_{\rm lrn}\rangle}(t)$ as the designed FF. Otherwise, go to Step 4.

Step 4: Estimate a plant FRF as $\hat{P}^{\langle i\rangle}(\omega_k)$ from the input/output data $u^{\langle i\rangle}(t)$ and $y^{\langle i\rangle}(t)$ of the plant and define the reliability function $W^{\langle i\rangle}(\omega_k)$.

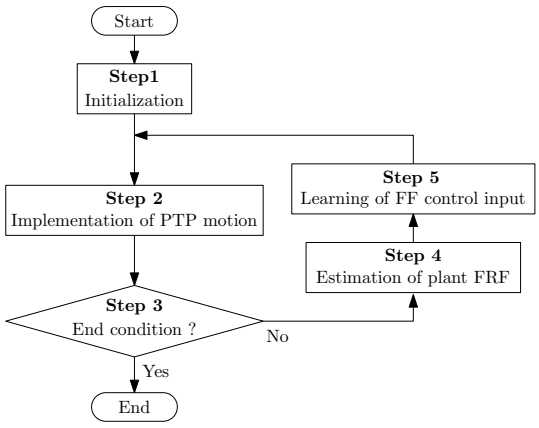

Fig. 4. Flowchart of MFILC-based FF design.

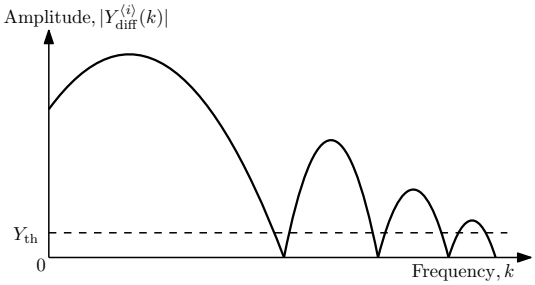

Fig. 5. Conceptual diagram of reliability evaluation.

Step 5: Update the learning filter $L^{\langle i\rangle}(\omega_k)$ and the robustness filter $Q^{\langle i\rangle}(\omega_k)$ using $\hat{P}^{\langle i\rangle}(\omega_k)$ and $W^{\langle i\rangle}(\omega_k)$ obtained in Step 4, and generate the DFT $U_{\rm ff}^{\langle i+1\rangle}(k)$ of FF control input $u_{\rm ff}^{\langle i+1\rangle}(t)$ for the next motion based on the learning law. Then, set $i := i+1$ and return to Step 2.

In Step 4, $W^{\langle i\rangle}(\omega_k)$ is defined considering the effect of disturbing noise $v^{\langle i\rangle}(t)$. Fig. 5 shows the conceptual diagram of the amplitude spectrum of DFT $Y_{\rm diff}^{\langle i\rangle}(k)$ of the differential output $y_{\rm diff}^{\langle i\rangle}(t)$ defined in Section III-C2. $Y_{\rm th}$ is the threshold of the disturbing noise effect. Typically, the DFT $R(k)$ of reference $r(t)$ does not exhibit sufficient spectral content at local frequencies and higher frequencies in PTP and reciprocating motion, which leads to almost zero spectral content in $Y_{\rm diff}^{\langle i\rangle}(k)$ at those corresponding frequencies. At around such frequencies, the disturbing noise effect tends to be greater in $Y_{\rm diff}^{\langle i\rangle}(k)$, and the reliability of $\hat{P}^{\langle i\rangle}(\omega_k)$ becomes low. Therefore, as the reliability evaluation algorithm, define $W^{\langle i\rangle}(\omega_k)$ by comparing $|Y_{\rm diff}^{\langle i\rangle}(k)|$ and $Y_{\rm th}$ as follows:

$$W^{\langle i\rangle}(\omega_k) := \begin{cases} 1 & : |Y_{\rm diff}^{\langle i\rangle}(k)| > Y_{\rm th} \\ W^{\langle i-1\rangle}(\omega_k) & : \text{Otherwise} \end{cases} \tag{4}$$

with $W^{\langle 0\rangle}(\omega_k) = 0,\ \forall\omega_k$.

B. MFILC

As is explained in Section III-A, the autonomous FF design method learns the FF control input $u_{\rm ff}^{\langle i\rangle}(t)$, through repeated execution of fixed PTP motion. Based on the general ILC manner, the DFT of FF control input is updated by the following learning law at every learning iteration [5], [8].

$$U_{\rm ff}^{\langle i+1\rangle}(k) := Q^{\langle i\rangle}(\omega_k)\{U_{\rm ff}^{\langle i\rangle}(k) + L^{\langle i\rangle}(\omega_k)E^{\langle i\rangle}(k)\} \tag{5}$$

with $u_{\rm ff}^{\langle 0\rangle}(t) = 0,\ \forall t$. According to the learning law of (5), the frequency-domain error $E^{\langle i+1\rangle}(k)$ at $(i+1)$-th learning iteration can be represented as

$$\begin{aligned} E^{\langle i+1\rangle}(k) = {} & \frac{1 - Q^{\langle i\rangle}(\omega_k)}{1 + C(\omega_k)P(\omega_k)}R(k) \\ & + Q^{\langle i\rangle}(\omega_k)\left\{1 - \frac{L^{\langle i\rangle}(\omega_k)P(\omega_k)}{1 + C(\omega_k)P(\omega_k)}\right\}E^{\langle i\rangle}(k) \end{aligned} \tag{6}$$

where $P(\omega_k)$ is the *unknown* plant FRF and $C(\omega_k)$ is the known FB controller FRF. Note that the effect of disturbing noise is neglected to simplify the discussion. From (6), when the following inequality condition is satisfied, the error decreases monotonically with each learning iteration.

$$\max\ \left|1 - \frac{L^{\langle i\rangle}(\omega_k)P(\omega_k)}{1 + C(\omega_k)P(\omega_k)}\right| < 1,\ \forall\omega_k \tag{7}$$

Here, in order to obtain fast convergence of the learning, it is desirable that $L^{\langle i\rangle}(\omega_k)$ satisfies ideally the following relationship [5], [10]–[12].

$$L^{\langle i\rangle}(\omega_k) = \frac{1 + C(\omega_k)P(\omega_k)}{P(\omega_k)},\ \forall\omega_k \tag{8}$$

Besides, $Q^{\langle i\rangle}(\omega_k)$ should be unity in a wide frequency range for fast convergence and fine tracking performance. Since the true $P(\omega_k)$ is *unknown* as stated in C3, it is difficult to define $L^{\langle i\rangle}(\omega_k)$ as (8). Therefore, in the conventional MFILC, $L^{\langle i\rangle}(\omega_k)$ and $Q^{\langle i\rangle}(\omega_k)$ are constructed according to the plant FRF estimate $\hat{P}^{\langle i\rangle}(\omega_k)$ and the reliability function $W^{\langle i\rangle}(\omega_k)$ as follows [10]:

$$\begin{aligned} L^{\langle i\rangle}(\omega_k) &:= \begin{cases} \dfrac{1 + C(\omega_k)\hat{P}^{\langle i\rangle}(\omega_k)}{\hat{P}^{\langle i\rangle}(\omega_k)} & : W^{\langle i\rangle}(\omega_k) = 1 \\ L^{\langle i-1\rangle}(\omega_k) & : W^{\langle i\rangle}(\omega_k) = 0 \end{cases} \\ Q^{\langle i\rangle}(\omega_k) &:= \begin{cases} 1 & : W^{\langle i\rangle}(\omega_k) = 1 \\ Q^{\langle i-1\rangle}(\omega_k) & : W^{\langle i\rangle}(\omega_k) = 0 \end{cases} \end{aligned} \tag{9}$$

with $L^{\langle -1\rangle}(\omega_k) = 0$ and $Q^{\langle -1\rangle}(\omega_k) = 0,\ \forall\omega_k$. In order to design the FF control input based on MFILC in a stable and efficient manner, as shown in (7) and (9), it is crucial to have an accurate estimation of the plant FRF in PTP motion.

C. FRF Estimation

1) ETFE: ETFE [6] is a simple FRF estimation method commonly used in many existing MFILC methods [9]–[12]. However, it cannot provide an accurate plant FRF estimate in PTP motion due to the non-periodic nature of input/output

data. From the state-space plant expression of (1), the DFT $Y^{\langle i\rangle}(k)$ of output data $y^{\langle i\rangle}(t)$ is formulated as follows:

$$Y^{\langle i\rangle}(k) = P(\omega_k)U^{\langle i\rangle}(k) + T^{\langle i\rangle}(\omega_k) + V^{\langle i\rangle}(\omega_k) \tag{10}$$

with

$$\begin{aligned} P(\omega_k) &= \boldsymbol{C}_{\rm p}(e^{j\omega_k T_{\rm s}}\boldsymbol{I} - \boldsymbol{A}_{\rm p})^{-1}\boldsymbol{B}_{\rm p} \\ T^{\langle i\rangle}(\omega_k) &= \boldsymbol{C}_{\rm p}(e^{j\omega_k T_{\rm s}}\boldsymbol{I} - \boldsymbol{A}_{\rm p})^{-1}e^{j\omega_k T_{\rm s}}\{\boldsymbol{x}_{\rm p}^{\langle i\rangle}(0) - \boldsymbol{x}_{\rm p}^{\langle i\rangle}(N)\} \end{aligned} \tag{11}$$

where $T^{\langle i\rangle}(\omega_k)$ is the leakage error and $V^{\langle i\rangle}(k)$ is the DFT of disturbing noise $v^{\langle i\rangle}(t)$. In ETFE, the plant FRF estimate $\hat{P}_{\rm ETFE}(\omega_k)$ is calculated as the ratio of $Y^{\langle i\rangle}(k)$ and $U^{\langle i\rangle}(k)$ as

$$\hat{P}_{\rm ETFE}^{\langle i\rangle}(\omega_k) := \frac{Y^{\langle i\rangle}(k)}{U^{\langle i\rangle}(k)} = P(\omega_k) + \frac{T^{\langle i\rangle}(\omega_k)}{U^{\langle i\rangle}(k)} + \frac{V^{\langle i\rangle}(k)}{U^{\langle i\rangle}(k)} \tag{12}$$

It is obvious from (12) that even if $V^{\langle i\rangle}(k) = 0$, $\hat{P}_{\rm ETFE}^{\langle i\rangle}(\omega_k)$ includes estimation errors when $T^{\langle i\rangle}(\omega_k) \neq 0$, and the leakage free condition under which $T_{\rm diff}(\Omega_k) = 0$ is derived as

$$\boldsymbol{x}_{\rm p}^{\langle i\rangle}(0) = \boldsymbol{x}_{\rm p}^{\langle i\rangle}(N) \tag{13}$$

As is stated as C4 in Section II, since (13) does not hold clearly in PTP motion ($\because \boldsymbol{x}_{\rm p}^{\langle i\rangle}(0) \neq \boldsymbol{x}_{\rm p}^{\langle i\rangle}(N)$), the FRF estimation error is inevitable in the conventional MFILC.

2) ETFE with Differential Filtering (ETFE-Diff): To overcome the aforementioned problem in ETFE-based FRF estimation, ETFE-Diff [15] is newly introduced to the proposed MFILC. In ETFE-Diff, first, the N-point time-domain differential input/output data $u_{\rm diff}^{\langle i\rangle}(t)$ and $y_{\rm diff}^{\langle i\rangle}(t)$ with $t = 0, 1, \ldots, N-1$ are calculated from the original data $u^{\langle i\rangle}(t)$ and $y^{\langle i\rangle}(t)$ as follows:

$$\begin{aligned} u_{\rm diff}^{\langle i\rangle}(t) &= u^{\langle i\rangle}(t) - u^{\langle i\rangle}(t-1) \\ y_{\rm diff}^{\langle i\rangle}(t) &= y^{\langle i\rangle}(t) - y^{\langle i\rangle}(t-1) \end{aligned} \tag{14}$$

Next, calculate the DFTs $U_{\rm diff}^{\langle i\rangle}(k)$ and $Y_{\rm diff}^{\langle i\rangle}(k)$ of $u_{\rm diff}^{\langle i\rangle}(t)$ and $y_{\rm diff}^{\langle i\rangle}(t)$. Finally, by dividing $Y_{\rm diff}^{\langle i\rangle}(k)$ by $U_{\rm diff}^{\langle i\rangle}(k)$ as same as ETFE, the plant FRF estimate $\hat{P}_{\rm ETFE-Diff}^{\langle i\rangle}(\omega_k)$ is defined by

$$\begin{aligned} \hat{P}_{\rm ETFE-Diff}^{\langle i\rangle}(\omega_k) &:= \frac{Y_{\rm diff}^{\langle i\rangle}(k)}{U_{\rm diff}^{\langle i\rangle}(k)} \\ &= P(\omega_k) + \frac{T_{\rm diff}^{\langle i\rangle}(\omega_k)}{U_{\rm diff}^{\langle i\rangle}(k)} + \frac{(1 - e^{-j\omega_k T_{\rm s}})V^{\langle i\rangle}(k)}{U_{\rm diff}^{\langle i\rangle}(k)} \end{aligned} \tag{15}$$

with

$$\begin{aligned} T_{\rm diff}^{\langle i\rangle}(\omega_k) &= \boldsymbol{C}_{\rm p}(e^{j\omega_k T_{\rm s}}\boldsymbol{I} - \boldsymbol{A}_{\rm p})^{-1}e^{j\omega_k T_{\rm s}} \\ &\quad \Big[\{\boldsymbol{x}_{\rm p}^{\langle i\rangle}(0) - \boldsymbol{x}_{\rm p}^{\langle i\rangle}(N)\} - \{\boldsymbol{x}_{\rm p}^{\langle i\rangle}(-1) - \boldsymbol{x}_{\rm p}^{\langle i\rangle}(N-1)\}\Big] \end{aligned} \tag{16}$$

where $T_{\rm diff}^{\langle i\rangle}(\omega_k)$ is the leakage error in ETFE-Diff and is expressed as a term of $\boldsymbol{x}_{\rm p}(t)$ with $t = -1, 0, N-1, N$ which is different from $T^{\langle i\rangle}(\omega_k)$ defined in (11) in ETFE. From (16), the leakage free condition in ETFE-Diff is derived as

$$\boldsymbol{x}_{\rm p}^{\langle i\rangle}(0) - \boldsymbol{x}_{\rm p}^{\langle i\rangle}(N) = \boldsymbol{x}_{\rm p}^{\langle i\rangle}(-1) - \boldsymbol{x}_{\rm p}^{\langle i\rangle}(N-1) \tag{17}$$

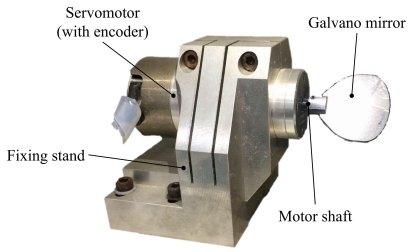

Fig. 6. Appearance of laboratory galvano scanner.

As stated as C4 in Section II, (17) holds in PTP motion that starts from and end to settled states and the leakage error can be successfully removed from the plant FRF estimate. In addition, (17) is also valid for periodic motion ($\boldsymbol{x}_{\rm p}^{\langle i\rangle}(0) = \boldsymbol{x}_{\rm p}^{\langle i\rangle}(N)$) including reciprocating motion as shown in Fig. 2(b). For details of theoretical analyses of ETFE-Diff, see [15].

It should be noted that, from (12) and (15), the plant FRF estimates in ETFE and ETFE-Diff are subject to estimation errors due to disturbing noise $V^{\langle i\rangle}(k)$. Therefore, in the MFILC, the effect of $V^{\langle i\rangle}(k)$ is removed based on the reliability evaluation algorithm in (4) as explained in Sections III-A and III-B.

IV. Simulation Evaluation

A. Target System

Fig. 6 exhibits a laboratory galvano scanner for laser processing of printed circuit boards [4]. A DC servomotor is utilized to control the angle of a galvano mirror that reflects a laser beam, with feeding back the motor angle y [rad/s] detected by a rotary encoder (resolution of 1.498×10^{-6} rad/pulse). The motor is driven through a current-controlled servo amplifier and the current reference is input to the amplifier as the control input u [V]. The control algorithm is calculated with the sampling time of $T_{\rm s} = 20$ μs in a DSP.

Black solid lines in Fig. 7 show the experimental plant FRF from u to y measured by sine sweep. The galvano scanner has two remarkable resonant modes at around 2.8 kHz and 6.0 kHz owing to the torsion of motor shaft and deflection of mirror. Therefore, taking into account the resonant characteristics, the following parametric plant model is established for the later simulation evaluation.

$$P(s) = K_{\rm a}e^{-L_{\rm a}s}\left(\frac{k_0}{s^2} + \sum_{h=1}^{2}\frac{k_h}{s^2 + 2\zeta_h\omega_h s + \omega_h^2}\right) \tag{18}$$

where $K_{\rm a}$ is the gain of servo amplifier, $L_{\rm a}$ is the equivalent dead time for the amplifier and D/A conversion, k_0 is the rigid mode gain, ω_h is the natural angular frequency of the h-th resonance mode, ζ_h is the h-th resonance mode damping coefficient, and k_h is the h-th resonance mode gain. In the later simulation, (18) is transformed to the discrete-time model considering the zeroth-order hold (sampling time of $T_{\rm s}$) as the true plant and its output angular position is quantized with resolution of 1.498×10^{-6} rad/pulse. The red dashed lines

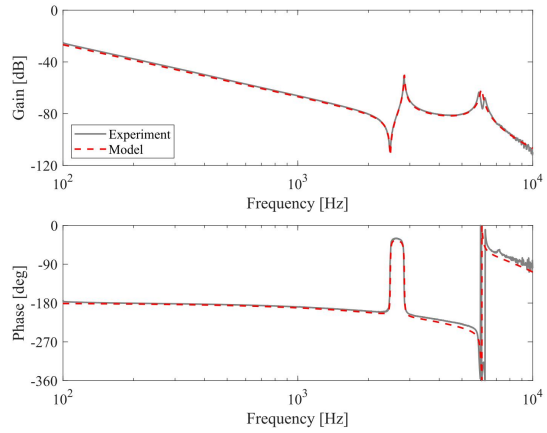

Fig. 7. Bode plots of plant model.

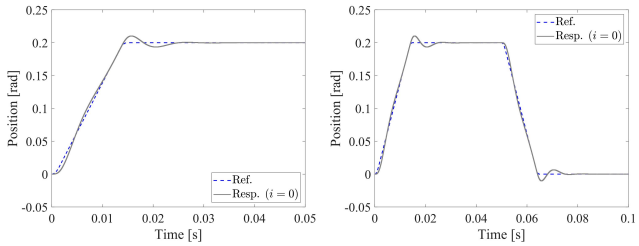

(a) (b)

Fig. 8. Waveforms of position reference $r(t)$: (a) PTP motion; (b) reciprocating motion.

in Fig. 7 show the FRF $P(\omega_k)$ that accurately reproduces the experimental FRF.

B. Settings of Simulation and MFILC

The MFILC-based automated FF design shown in Fig. 3 is constructed on MATLAB/Simulink and simulation evaluations are performed. In this study, two-type angular position references $r(t)$, namely PTP motion and reciprocating motion as depicted by blue dashed lines in Fig. 8, were employed to validate the efficacy of the proposed ETFE-Diff-based MFILC. $r(t)$ was designed as the S-shape trajectory with the position stroke of 0.2 rad, the maximum velocity of ± 15 rad/s, and the maximum acceleration of ± 10000 rad/s^2, considering a typical laser processing motion. Note that, for estimating the plant FRF with a sufficient frequency resolution, zero-padding was applied to the end of M-point time-domain data obtained by each motion to make the total data length $N = 16384$. In this study, set $M = 2500$ ($2500T_\mathrm{s} = 0.05$ s) in PTP motion and $M = 5000$ ($5000T_\mathrm{s} = 0.10$ s) in reciprocating motion, respectively. For simplicity, a PID controller was selected as the FB controller C and its proportional, integral, and derivative gains were manually designed beforehand to ensure a large stability margin (i.e., a low control bandwidth) under the assumption that the true plant FRF is *unknown* as stated in C3. The position responses before applying the MFILC-based FF design are depicted by black solid lines in Fig. 8. The position tracking performance is severely compromised in the absence of FF compensation.

The setting parameters in MFILC are Y_th for determining the reliability of plant FRF estimate and the number of learning iteration times N_lrn. Y_th was set to $Y_\mathrm{th} = 0.001$, considering the equivalent noise due to the quantization of detected angular position. If the level of the disturbing noise is measured or known beforehand, determining Y_th can be straightforward [10]. On the other hand, N_lrn was set to $N_\mathrm{lrn} = 10$ by trial-and-error to achieve sufficient convergence during learning.

C. Simulation Results

1) PTP Motion: The simulation results of the conventional and proposed methods in PTP motion are respectively shown in Fig. 9 and Fig. 10. For visibility of the figures, time-domain results are depicted only for $i = 0, 1,$ and 10, while frequency-domain results are displayed only for $i = 0, 1,$ and 9. In the case of the conventional method, as explained theoretically in Section III-C1, the ETFE-based FRF estimation causes leakage error in PTP motion, and thus the plant FRF estimate $\hat{P}^{\langle i \rangle}(\omega_k)$ includes significant errors compared to the true plant FRF $P(\omega_k)$. This is shown in Fig. 9(c) and Fig. 9(d). As a result, the FF control input $u_\mathrm{ff}^{\langle i \rangle}(t)$ cannot be learned appropriately as shown in Fig. 9(b), and the position error $e^{\langle i \rangle}(t)$ diverges by repeating learning as shown in Fig. 9(a) and Fig. 9(e). On contrast, in the case of the proposed method, the plant FRF estimate accuracy gradually improves as the learning iteration increases as shown in Fig. 10(c) and Fig. 10(d), and the position error is successfully reduced by the learned $u_\mathrm{ff}^{\langle i \rangle}(t)$ as shown in Fig. 10(a), Fig. 10(b), and Fig. 10(e). The FRF estimation errors in the higher frequencies are due to the fact that the position reference $r(t)$ shown in Fig. 8 does not have sufficient frequency components in those frequencies.

In order to confirm the principle of the proposed MFILC, the learning filter $L^{\langle i \rangle}(\omega_k)$ when $i = 0, 1, 3,$ and 9 are shown in Fig. 11. When $i = 0$ shown in Fig. 11(a), since the position response was very slow due to $u_\mathrm{ff}^{\langle 0 \rangle}(t) = 0$, the reliability of $\hat{P}^{\langle 0 \rangle}(\omega_k)$ was limited under 430 Hz, resulting that $L^{\langle 0 \rangle}(\omega_k)$ matched the ideal $L(\omega_k)$ defined as (8) under 430 Hz. When $i \geq 1$, by repetitively learning the FF control input from $L^{\langle i-1 \rangle}(\omega_k)$ (and the corresponding $Q^{\langle i-1 \rangle}(\omega_k)$), a faster position response could be obtained and the reliability of $\hat{P}^{\langle i \rangle}(\omega_k)$ extended to a higher frequency range. Finally, $L^{\langle 9 \rangle}(\omega_k)$ well reproduced the ideal $L(\omega_k)$ by 555 Hz, hence the fine control performance shown in Fig. 10 could be achieved.

2) Reciprocating Motion: The simulation results of the proposed method in reciprocating motion are presented in Fig. 12. These results demonstrate that the proposed method achieves accurate FF compensation not only in PTP motion but also in reciprocating motion. Therefore, the proposed ETFE-Diff-based MFILC can extend the range of learnable operating conditions beyond what is possible with conventional MFILC methods [9]–[12] (i.e., the leakage free condition is extended from (13) to (17)), which has potential advantages for industrial applications. It should be noted that although the

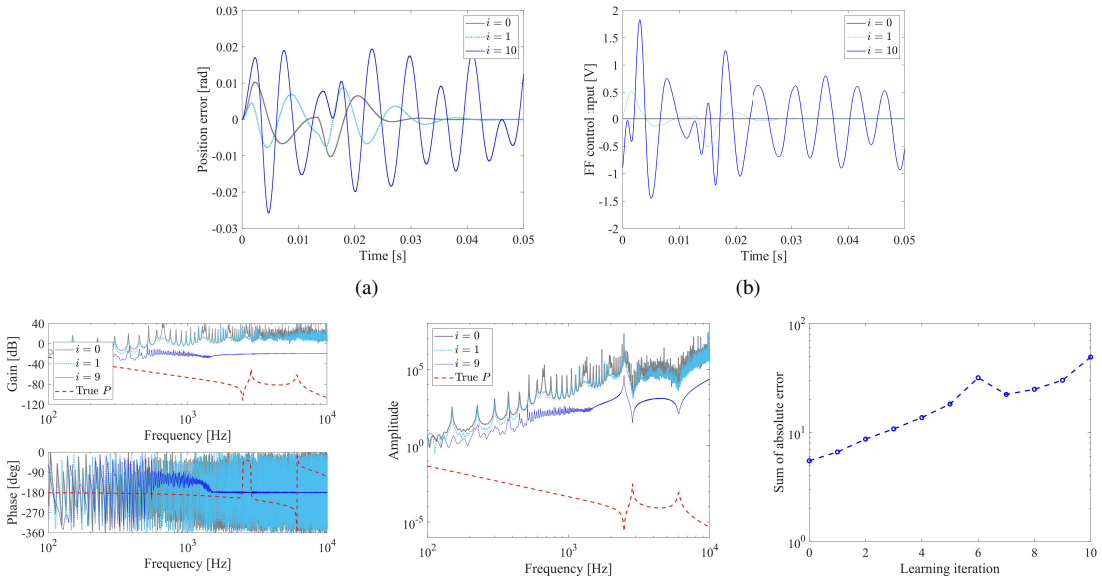

Fig. 9. Simulation results of **conventional method** in **PTP motion**: (a) position error $e^{\langle i \rangle}(t)$; (b) FF control input $u_{\mathrm{ff}}^{\langle i \rangle}(t)$; (c) plant FRF estimate $\hat{P}^{\langle i \rangle}(\omega_k)$; (d) FRF estimate error $|P(\omega_k) - \hat{P}^{\langle i \rangle}(\omega_k)|/|P(\omega_k)|$; (e) sum of absolute error $|e^{\langle i \rangle}(t)|$.

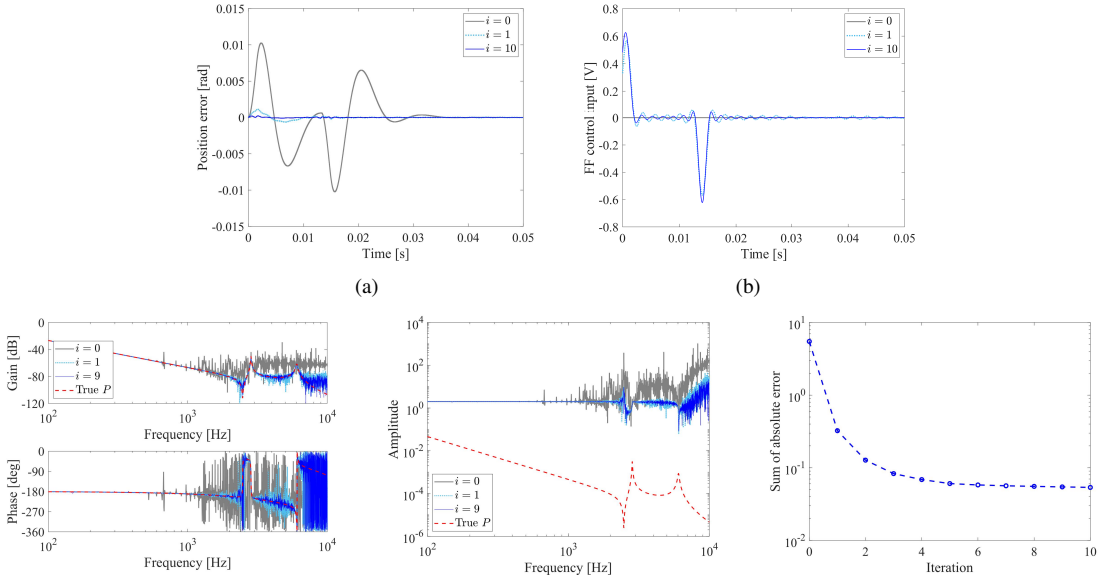

Fig. 10. Simulation results of **proposed method** in **PTP motion**: (a) position error $e^{\langle i \rangle}(t)$; (b) FF control input $u_{\mathrm{ff}}^{\langle i \rangle}(t)$; (c) plant FRF estimate $\hat{P}^{\langle i \rangle}(\omega_k)$; (d) FRF estimate error $|P(\omega_k) - \hat{P}^{\langle i \rangle}(\omega_k)|/|P(\omega_k)|$; (e) Sum of absolute error $|e^{\langle i \rangle}(t)|$.

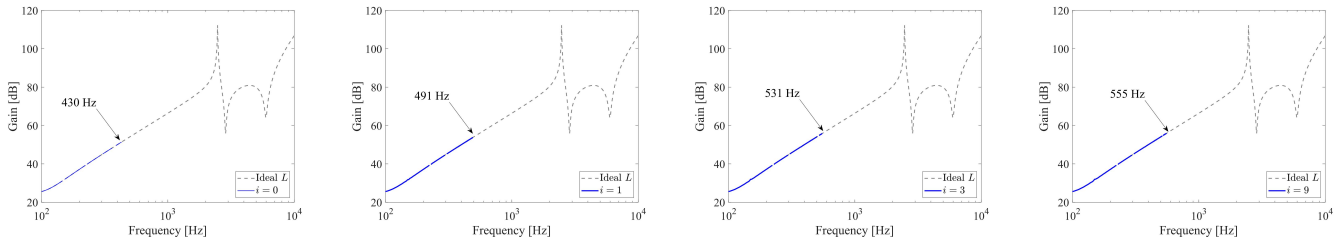

Fig. 11. Learning filter $L^{\langle i \rangle}(\omega_k)$ of **proposed method** when $i = 0, 1, 3, 9$ in **PTP motion**.

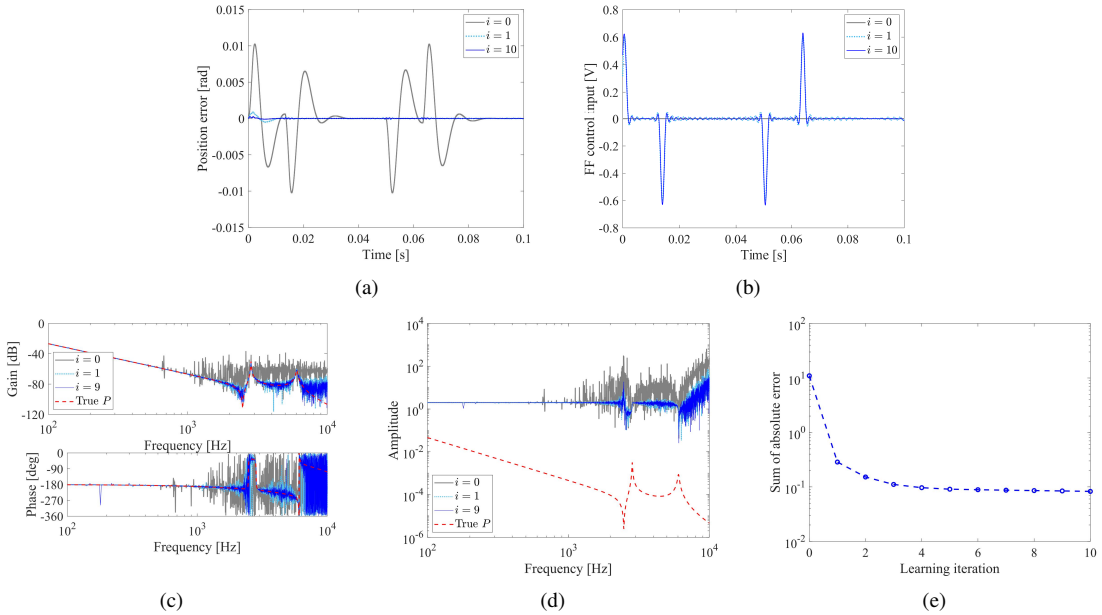

Fig. 12. Simulation results of **proposed method** in **reciprocating motion**: (a) position error $e^{\langle i \rangle}(t)$; (b) FF control input $u_{\mathrm{ff}}^{\langle i \rangle}(t)$; (c) plant FRF estimate $\hat{P}^{\langle i \rangle}(\omega_k)$; (d) FRF estimate error $|P(\omega_k) - \hat{P}^{\langle i \rangle}(\omega_k)|/|P(\omega_k)|$; (e) sum of absolute error $|e^{\langle i \rangle}(t)|$.

results of the conventional method in reciprocating motion are not included in this paper due to space constraints, the conventional method also achieved satisfactory performance in this type of motion.

V. Conclusions

We have presented an improved frequency-domain MFILC method that can automatically design FF compensation for achieving fine motion control performance in both reciprocating and PTP motion. The proposed method employs ETFE-Diff-based FRF estimation, which allows for expanded learnable operating conditions compared to the conventional MFILC. The theoretical principles and algorithm of the proposed MFILC were described in detail, and simulations were conducted to demonstrate its effectiveness in achieving fast and precise motion control of the galvano scanner. The proposed method can have practical advantages in industrial applications, such as directly learning to design FF for PTP motion.

References

[1] Y. Wu and Q. Zou, "Robust Inversion-Based 2-DOF Control Design for Output Tracking: Piezoelectric-Actuator Example," *IEEE Trans. Control Syst. Technol.*, vol. 17, no. 5, pp. 1069–1082, 2009.

[2] M. Iwasaki, K. Seki, and Y. Maeda, "High-Precision Motion Control Techniques – A Promising Approach to Improving Motion Performance," *IEEE Ind. Electron. Mag.*, vol. 6, no. 1, pp. 32–40, 2012.

[3] H. Fujimoto, Y. Hori, and A. Kawamura, "Perfect Tracking Control Based on Multirate Feedforward Control With Generalized Sampling Periods," *IEEE Trans. Ind. Electron.*, vol. 48, no. 3, pp. 636–644, 2001.

[4] Y. Maeda and M. Iwasaki, "Improvement of Adaptive Property by Adaptive Deadbeat Feedforward Compensation Without Convex Optimization," *IEEE Trans. Ind. Electron.*, vol. 62, no. 1, pp. 466–474, 2015.

[5] D.A. Bristow, M. Tharayil, and A.G. Alleynek, "A Survey of Iterative Learning Control," *IEEE Control Syst. Mag.*, vol. 26, no. 3, pp. 96–114, 2006.

[6] J. Schoukens, K. Godfrey, and M. Schoukens, "Nonparametric Data-Driven Modeling of Linear Systems," *IEEE Control Syst. Mag.*, pp. 49–88, 2018.

[7] Y. Maeda, K. Harata, and M. Iwasaki, "A Friction Model-Based Frequency Response Analysis for Frictional Servo Systems," *IEEE Trans. Ind. Inform.*, vol. 14, no. 11, pp. 5246–5255, 2018.

[8] Y. Chen and K.L. Moore, "An Optimal Design of PD-type Iterative Learning Control With Monotonic Convergence," in *Proc. 2002 IEEE Int. Symp. Intell. Control*, 2002, pp. 55–60.

[9] S. Tien, Q. Zou, and S. Devasia, "Iterative Control of Dynamics-Coupling-Caused Errors in Piezoscanners During High-Speed AFM Operation," *IEEE Trans. Control Syst. Technol.*, vol. 13, no. 6, pp. 921–931, 2005.

[10] K.-S. Kim and Q. Zou, "A Modeling-Free Inversion-Based Iterative Feedforward Control for Precision Output Tracking of Linear Time-Invariant Systems," *IEEE/ASME Trans. Mechatron.*, vol. 18, no. 6, pp. 1767–1777, 2018.

[11] R. de Rozario, A. Fleming, and T. Oomen, "Finite-Time Learning Control Using Frequency Response Data With Application to a Nanopositioning Stage," *IEEE/ASME Trans. Mechatron.*, vol. 24, no. 5, pp. 2085–2096, 2019.

[12] R. de Rozario and T. Oomen, "Data-Driven Iterative Inversion-Based Control: Achieving Robustness Through Nonlinear Learning," *Automatica*, vol. 107, Sep., pp. 342–353, 2019.

[13] Z. Wang and Q. Zou, "A Modeling-Free Differential-Inversion-Based Iterative Learning Control Approach to Simultaneous Hysteresis-Dynamics Compensation: High-Speed Large-Range Motion Tracking Example," in *Proc. 2015 American Control Conf.*, 2015, pp. 3558–3563.

[14] R. de Rozario and T. Oomen, "Learning Control Without Prior Models: Multi-Variable Model-Free IIC, with Application to a Wide-Format Printer," in *Proc. 8th IFAC Symp. Mechatron. Syst.*, 2019, pp. 366–371.

[15] Y. Maeda and M. Iwasaki, 'Empirical Transfer Function Estimation with Differential Filtering and Its Application to Fine Positioning Control of Galvano Scanner," *IEEE Trans. Ind. Electron.*, vol. 70, no. 10, pp. 10466–10475, 2023.

[16] Y. Maeda, H. Tachibana, and M. Iwasaki, "Comparative Evaluations of Frequency Response Analysis Methods for Fast and Precise Point-To-Point Position Control," in *Proc. 15th IEEE Int. Workshop Adv. Motion Control*, pp. 437–442, 2018.